Stochastic 16-State Model of Voltage Gating of Gap-Junction Channels Enclosing Fast and Slow Gates

Nerijus Paulauskas,[†¶] Henrikas Pranevicius,[‡] Jonas Mockus,[§] and Feliksas F. Bukauskas[†*]
[†]Dominick P. Purpura Department of Neuroscience, Albert Einstein College of Medicine, New York, New York; [‡]Department of Business Informatics, Kaunas University of Technology, Kaunus, Lithuania; [§]Department of Systems Analysis, Institute of Mathematics and Informatics, Vilnius University, Vilnius, Lithuania; and [¶]Institute of Cardiology, Lithuanian University of Health Sciences, Kaunas, Lithuania

ABSTRACT Gap-junction (GJ) channels formed of connexin (Cx) proteins provide a direct pathway for electrical and metabolic cell-cell interaction. Each hemichannel in the GJ channel contains fast and slow gates that are sensitive to transjunctional voltage (V_j). We developed a stochastic 16-state model (S16SM) that details the operation of two fast and two slow gates in series to describe the gating properties of homotypic and heterotypic GJ channels. The operation of each gate depends on the fraction of V_j that falls across the gate (V_G), which varies depending on the states of three other gates in series, as well as on parameters of the fast and slow gates characterizing 1), the steepness of each gate's open probability on V_G; 2), the voltage at which the open probability of each gate equals 0.5; 3), the gating polarity; and 4), the unitary conductances of the gates and their rectification depending on V_G. S16SM allows for the simulation of junctional current dynamics and the dependence of steady-state junctional conductance ($g_{j,ss}$) on V_j. We combined global coordinate optimization algorithms with S16SM to evaluate the gating parameters of fast and slow gates from experimentally measured $g_{j,ss}$-V_j dependencies in cells expressing different Cx isoforms and forming homotypic and/or heterotypic GJ channels.

INTRODUCTION

Connexins (Cxs), a large family of membrane proteins, form gap junction (GJ) channels that provide a direct pathway for electrical and metabolic signaling between cells. Each GJ channel is composed of two hemichannels, oligomers of six Cxs. Gap-junctional communication plays important roles in many processes, such as impulse propagation in the heart, communication between neurons and glia, metabolic exchange between cells in the lens and other tissues lacking blood circulation, organ formation during development, and regulation of cell proliferation (1–3).

A property that appears to be common to GJ channels formed by any Cx isoform is the sensitivity of junctional conductance (g_j) to transjunctional voltage (V_j) (1,3,4). The symmetric reduction in g_j with positive or negative V_j has been explained by having V_j-sensitive gate/s in each apposed/junctional hemichannel (aHC). A common feature of V_j gating is that steady-state g_j ($g_{j,ss}$) does not decline to zero with increasing V_j, but instead reaches a residual or minimal conductance (g_{min}). Single-channel studies have shown that g_{min} is due at least in part to incomplete closure of the GJ channel by V_j, i.e., V_j causes channels to close to a subconductance (residual) state with fast gating transitions ($\sim \leq 1$ ms) (5,6). It was shown that V_j as well as chemical uncouplers can also induce gating transitions to the fully closed state, and that these transitions are slow (~10 ms) (7,8). Gating to different levels via distinct fast and slow gating transitions led to the suggestion that there are two distinct V_j sensitive gates, termed fast and slow (or loop) gating mechanisms (2).

In earlier studies, Harris (4) described the gating properties of GJ channels by using the Boltzmann function and assuming that GJ channels have two states (open and fully closed) like most ionic channels. Such an approach allowed for the description of gating properties of GJs assuming that each hemichannel gates independently. Other authors attempted to describe V_j gating of GJs by using a four-state model in which each hemichannel contained a fast gate operating between open and residual states (9,10). Both models made significant progress by introducing a more detailed description of GJ channels based on the latest experimental data at the time. However, neither of these models allowed the kinetics of junctional current (I_j) to be studied during applied transjunctional voltages. Furthermore, a three-state model of V_j gating was proposed that was adapted to GJs that demonstrate multiple substates (11).

Here, we present a stochastic 16-state model (S16SM) of V_j gating. Each aHC contains both fast and slow gating mechanisms. Each gate can be in open or closed states that exhibit I/V rectification. The model was used to simulate experimental data of V_j gating in homotypic and heterotypic junctions. S16SM allowed us to simulate the dynamics of I_j as well as a $g_{j,ss}$-V_j plot of GJs depending on individual gating parameters of four gates and variation of the open probability of each gate over time. We combined global coordinate optimization (GCO) algorithms with S16SM to evaluate the gating parameters of fast and slow gates from experimentally measured $g_{j,ss}$-V_j dependencies in cells expressing different Cx isoforms.

Submitted February 14, 2012, and accepted for publication April 25, 2012.

*Correspondence: feliksas.bukauskas@einstein.yu.edu

Editor: Chris Lingle.

0006-3495/12/06/2471/10 $2.00

doi: 10.1016/j.bpj.2012.04.038

MATERIALS AND METHODS

Cells and culture conditions

Experiments were performed with HeLa cells (human cervix carcinoma cells, ATCC CCL2) stably transfected with different Cx isoforms. Cells were grown in Dulbecco's modified Eagle's medium. More details about the DNAs used for transfection and selection of clones stably expressing different Cx isoforms can be found in Bukauskas et al. (12).

Electrophysiological measurements

Experiments were performed in modified Krebs-Ringer (MKR) solution containing (in mM) NaCl, 140; KCl, 4; $CaCl_2$, 2; $MgCl_2$, 1; glucose, 5; Na pyruvate, 2; and HEPES, 5 (pH 7.4). Patch electrodes were filled with a pipette solution containing (in mM) KCl, 130; NaAsp, 10; MgATP, 3; $MgCl_2$, 1; $CaCl_2$, 0.2; EGTA, 2; and HEPES, 5 (pH = 7.2). For electrophysiological recordings, cells were grown on glass coverslips and transferred to an experimental chamber mounted on the stage of an inverted microscope (Olympus IX70). The cells were perfused with MKR solution at room temperature. Junctional conductance (g_j) was measured in selected cell pairs by means of a dual whole-cell patch-clamp system (13). Briefly, each cell within a pair was voltage-clamped with a patch-clamp amplifier (EPC-7plus; HEKA, Bellmore, NY). Transjunctional voltage (V_j) was induced by stepping the voltage in one cell (cell 1, ΔV_1) and keeping the other constant, $V_j = \Delta V_1$. Junctional current (I_j) and g_j ($g_j = I_j/V_j$) were measured as the change in current in the unstepped cell (cell 2, $I_j = \Delta I_2$). Signals were acquired and analyzed with the use of custom-made software (14).

RESULTS

Physiology of fast and slow gates

Demonstration of fast and slow gates required us to consider four rather than two gates as we did in the model describing gating of GJs (15). In this case, it is important to use the most recent information about the functional properties of fast and slow gates. The starting hypothesis about fast and slow gating mechanisms was based on recordings of de novo GJ channel formation observed after initiating contact between two patched insect cells (*Aedes albopictus*, clone C6/36) (5,16). The first opening events of GJs occurred within a short time (~30 s) and exhibited relatively slow junctional current transitions (~10–50 ms) from the closed to the open state (~365 pS) followed by fast gating transitions (<~1 ms) between the open state and the substate, called a residual state, with conductance of ~64 pS. On the basis of these data, Bukauskas and Weingart (5) concluded that "gap junctions possess two gates, a fast gate controlled by V_j and giving rise to γ_j (residual), and a slow gate…able to close the channel completely." Furthermore, gating of GJs to the substate and two distinct types of gating transitions were reported in mammalian cells expressing different Cx isoforms (2,3,6,7,17,18), and it was shown that the slow gate is also sensitive to V_j (8,12). Two types of gating transitions were also observed under an effect of V_j combined with chemical uncouplers, e.g., acidification, as illustrated in Fig. 1 *A*, which typically leads to full uncoupling. Two distinct gating mechanisms were also demonstrated in Cx-based unapposed/nonjunctional hemichannels (uHC) (14). Fast and slow gating mechanisms can have the same gating polarity or different polarities. For example, in Cx45 and Cx43, both gates tend to close at negativity (19), whereas in Cx46 uHCs the fast and slow gates close at positivity and negativity, respectively, on their cytoplasmic side (14). Together, these data allow the conclusion that indeed each hemichannel of the GJ channel possesses two fast and two slow gates operating in series (Fig. 1 *B*). They are spatially separated and interact through changes of electrical field across each

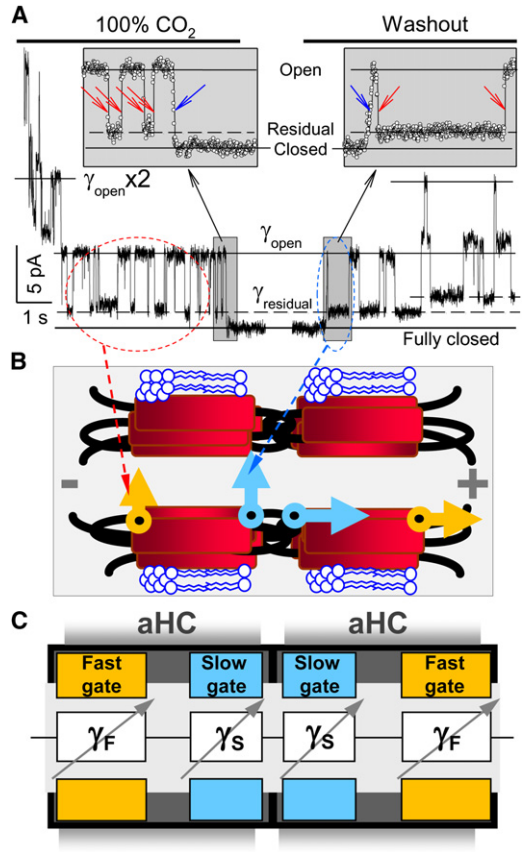

FIGURE 1 GJ channels contain fast and slow gating mechanisms. (*A*) Effect of CO_2 on voltage gating at the single-channel level in a fibroblast cell pair expressing Cx43. Exposure to 100% CO_2 causes full uncoupling. I_j was monitored at V_j = 55 mV just before full uncoupling and at the beginning of washout of CO_2. Channels exhibited two types of I_j transition: 1), between open and residual states (~90 pS), with a transition time of ~1–2 ms (*red arrows*); and 2), between open and fully closed states (~120 pS), with a transition time of ~10 ms (*blue arrows*). The signals in the insets (sampled at 1 ms interval) illustrate that the last channel closes with a transition time of ~10 ms and the first channel opens with a transition time of ~19 ms. The slow opening of the first channel during washout is followed by fast flickering between open and residual states. When two operating channels are in the residual state, g_j equals the sum of two γ_{res} (*dashed lines*; modified from Fig. 1 in Bukauskas and Peracchia (7)). (*B*) Schematic of the GJ channel illustrating which gate operates during fast and slow gating transitions. The fast gate (*orange*) closes the channel partially, and the slow gate (*blue*) closes it fully. (*C*) The schematic of the GJ channel is combined with the principal electrical scheme composed of four variable resistances in series attributed to fast (γ_F) and slow (γ_S) gates.

gate (V_G) depending on the state of other three gates in series (2).

Description of the model

In the model, each gate is characterized by its gating polarity and the unitary conductances of the open (γ_{open}) and closed (γ_{closed}) states. The slow gate fully closes the channel ($\gamma_{S,closed} = 0$), and the fast gate closes the channel to the residual state ($\gamma_{F,closed} = \gamma_{F,res}$), which is ~1/5 of the open state (2) (Fig. 1 *C*). In the stochastic four-state model (S4SM), we assumed, based on an earlier attempt to simulate $g_{j,ss}$-V_j dependence (10), that each hemichannel contains one gate that can be open (*o*) or closed (*c*). Then, the channel can occupy one of four possible states: *o-o* (both gates open), *c-c* (both gates closed), *c-o* (one gate open), and *o-c* (one gate closed). Therefore, the channel can be in four states as shown in Fig. S1 *A* of the Supporting Material, where K_i ($i = 1, 2, 3, 4$) are equilibrium constants for transitions between states. In S4SM, we used a stochastic approach to describe the operation of each gate, which allowed us to simulate changes of I_j and g_j over time and $g_{j,ss}$-V_j dependence. This model is available online (http://connexons.aecom.yu.edu/Applet.htm), and its application in analyzing gating of GJs under normal and pathological conditions is described elsewhere (20–22).

Here, we report a model of V_j gating of GJs containing in series one fast and one slow gate with conductances of $\gamma_{F,open}$ and $\gamma_{S,open}$, respectively, in each aHC. The fast gate closes to the residual state with conductance $\gamma_{F,res}$, whereas the slow gate closes channels fully, $\gamma_{S,closed} = 0$. The $\gamma_{F,open}$, $\gamma_{F,res}$, and $\gamma_{S,open}$ will be the same in both aHCs of homotypic GJ channels and different in aHCs of heterotypic GJ channels. The model follows Markov's principle, i.e., the probability of transitions does not depend on the history of previous transitions. When each aHC contains two gates (Fig. S1 *B*), each state of the fast gates can combine with four states of the slow gates. Therefore, the GJ channel can be in 16 different states, resulting in a stochastic 16-state model, S16SM. An equilibrium constant between open and closed/residual states of slow ($K_{S,o\leftrightarrow c}$) and fast ($K_{F,o\leftrightarrow r}$) gates will be determined by the fraction of V_j across each gate, V_S and V_F, in a similar fashion as for S4SM, i.e., $K_{S,o\leftrightarrow c} = e^{A_S\cdot(-\Pi\cdot V_S - V_{S,o})}$ and $K_{F,o\leftrightarrow res} = e^{A_F\cdot(-\Pi\cdot V_F - V_{F,o})}$, where A_F and A_S characterize sensitivity to voltage, $V_{F,o}$ and $V_{S,o}$ are voltages at which $K_{S,o\leftrightarrow c}$ and $K_{F,o\leftrightarrow res}$ are equal to 1, and Π is a gating polarity (+1 or −1). The model also accounts for rectification of $\gamma_{S,open}$, $\gamma_{F,open}$, and $\gamma_{F,res}$, which is described as an exponential function as proposed previously (9), e.g., $\gamma_{F,res} = \gamma_{F,res,0}\cdot e^{-V_F/R_{F,res}}$, where $\gamma_{F,res,0}$ is $\gamma_{F,res}$ at $V_F = 0$ and $R_{F,res}$ is the rectification coefficient of the residual state.

Several studies have demonstrated the rectification of open and residual conductances of uHCs and GJ channels (13,14,19,23). It was proposed that the I/V rectification results from the number and position of charged residues along the channel pore and can be described using an electrodiffusive model derived from the Poisson-Nernst-Plank equation (23). The primary source for the rectification of γ_{open} and γ_{res} of GJs is the rectification of $\gamma_{F,open}$, $\gamma_{F,res}$, and $\gamma_{S,open}$. Transjunctional voltage across the GJ channel is a sum of voltages across all gates, $V_j = V_{F,A} + V_{S,A} + V_{F,B} + V_{S,B}$, where A and B stand for aHCs A and B. Closing one gate changes the voltage not only across this gate but also across the other three gates in series, and this will affect the probability of changing the state over a discrete time interval Δt.

The presence of $\gamma_{F,open}$, $\gamma_{F,res}$, and $\gamma_{S,open}$ rectification does not allow for the evaluation of voltages across individual gates, V_G, in one step, and requires recalculation of the gates' conductances until a conditional steady state is approached. In brief, at an initial moment of a discrete time interval, we know the states of each gate as well as V_j, which allows us to estimate the voltages across each gate without accounting for rectification. Then, using these voltages, we recalculate the conductances of gates while accounting for rectification, and consequently reevaluate a new set of voltages across them. We repeat this process several times, and each time evaluate the conductance of the GJ channel (γ_j) as well as the difference, $\Delta\gamma_{j,n} = \gamma_{j,n+1} - \gamma_{j,n}$. To avoid an infinite loop ($n \rightarrow \infty$), we define the tolerance criteria $e = \gamma_{j,o}/10{,}000$, and at $\Delta\gamma_j < e$ we stop the cycling process and define the final values of V_Gs, which allows us to evaluate possible changes in the state of each gate. This information is transferred to the next discrete time interval and the above-described process is repeated. In all calculations, n is in the range of 2–7. If condition $\Delta\gamma_j < e$ is not satisfied, the cycling stops at $n = 10$. Fig. S2 shows an example of a γ_j–n plot demonstrating that γ_j reaches steady state relatively quickly.

In the algorithm that describes V_j gating, we assume that gates do not interact with each other except via voltage redistribution inside the pore, and only the transgate voltage defines the gate's $o \leftrightarrow c$ transitions. Then, the probabilities of each gate can be defined as reported earlier (10,15) by equilibrium constants (K), e.g., for the fast gate $K_F = P_{o\rightarrow c} / P_{c\rightarrow o}$. We define a discrete time interval, Δt, during which only one transition for each gate is possible. Interval Δt is used as a simulation step. For example, when $K_F = 1$, both open and closed states of the fast gate are equally possible, $P_o = P_c$. When the system is at equilibrium, the average number of open and closed gates does not change. Thus, the average number of opening and closing events of the gate must be equal, i.e., $P_o\cdot P_{o\rightarrow c} = P_c\cdot P_{c\rightarrow o}$. If we label $P\tau$ as the probability that the gate will change its state during time interval Δt, then $P\tau = P_o\cdot P_{o\rightarrow c} + P_c\cdot P_{c\rightarrow o}$. When both states are equally probable ($K_F = 1$), then $P_o = P_c = 1/2$ and $P\tau = (P_{o\rightarrow c} + P_{c\rightarrow o})/2$. The difference, $1 - P\tau$, is the probability that the gate will stay in the same state. In general, the model defines at any given time

whether an individual gate will remain in the same state or change its state. In a junction composed of thousands of GJ channels, any new calculation at the same V_j protocol results in a random distribution of open and closed states over time for individual channels, whereas the mean g_j remains the same.

S16SM includes the unitary conductances of gates in open and closed/residual states ($\gamma_{F,open}$, $\gamma_{S,open}$, and $\gamma_{F,res}$) and their rectification, which cannot be measured directly but is approximated from rectification of γ_{open} and γ_{res} measurements in GJs and uHCs or estimated during global optimization (see below). In general, γ of the GJ channel in the model follows from the connection in series of four variable conductances defined by the state of each gate as well as by V_G, if gates exhibit I/V rectification.

Simulation of voltage gating in homotypic GJs at the macroscopic/multichannel level

We combined S16SM with two types of stimulation protocols used most frequently in experiments: 1), consecutive V_j steps that increase in amplitude, and measuring I_j at the end of V_j steps when it reaches a steady-state level; and 2), slowly raising V_j ramps that allow I_j to reach a steady state continuously over the entire V_j range. Fig. 2, *A–F*, shows the simulation of V_j gating in a junction containing 3000 hypothetical GJ channels during a series of V_j steps that varied from −120 to 120 mV every 10 mV (Fig. 2 *A*). We assume that the conductance of the single GJ channel is 110 pS, which is within the range of γ_{open} values of different Cx isoforms (~10–300 pS (2,3)) and identical to γ_{open} of Cx43 (12). There are no reported data on $\gamma_{F,open}$, $\gamma_{S,open}$, and $\gamma_{F,res}$, and for simplicity we assumed that the conductance of each of four gates at the open state is 440 pS (110 pS × 4). This value follows from a postulate that the diameter of the pore in regions of both gates in the open state, as well as their lengths, are approximately the same and therefore $\gamma_{F,open} = \gamma_{S,open}$. Single GJ channel conductance measured experimentally in homotypic GJ channels can be related to conductances of four gates as follows: $1/\gamma_{open} = 2/\gamma_{F,open} + 2/\gamma_{S,open}$ or $\gamma_{F,open} = \gamma_{S,open} = 4\ \gamma_{open}$. The residual conductance of the GJ channel typically is ~1/5 of γ_{open} (2), i.e., $\gamma_{res} = 110/5 = 22$ pS, which is measured when one of the fast gates is in the residual state and three other gates in series are open ($1/\gamma_{res} = 1/\gamma_{F,res} + 1/\gamma_{F,open} + 2/\gamma_{S,open}$). From here, we can find that $\gamma_{F,res}$ should be equal 25.9 pS. Therefore, the ratio between conductances in the open and residual states of the fast gate is 3.4-fold higher than that of the GJ channel ($\gamma_{F,open}/\gamma_{F,res} = 440/25.9 = 17$ vs. $\gamma_{open}/\gamma_{res} = 5$). In addition, we assume that $\gamma_{F,res}$, $\gamma_{F,open}$, and $\gamma_{S,open}$ rectify (i.e., their values change exponentially depending on the transgate voltage, as shown in Fig. 2 *D*). The hypothetical values of rectification coefficients ($R_{F,open}$, $R_{F,res}$, and $R_{S,open}$) and parameters characterizing sensitivity to V_j of fast and slow gates ($V_{F,o}$, $V_{S,o}$, A_F, and A_S) are shown in Table S1. These values are within the range of estimates we made using global optimization (see below) of different Cxs. Fig. 2, *B* and *C*, show a family of I_j and g_j traces for all applied V_j steps. Fig. 2 *E* shows averaged open probabilities of fast and slow gates in hemichannels A and B depending on V_j. Fig. 2 *F* shows conductance changes of A ($g_{H,A}$) and B

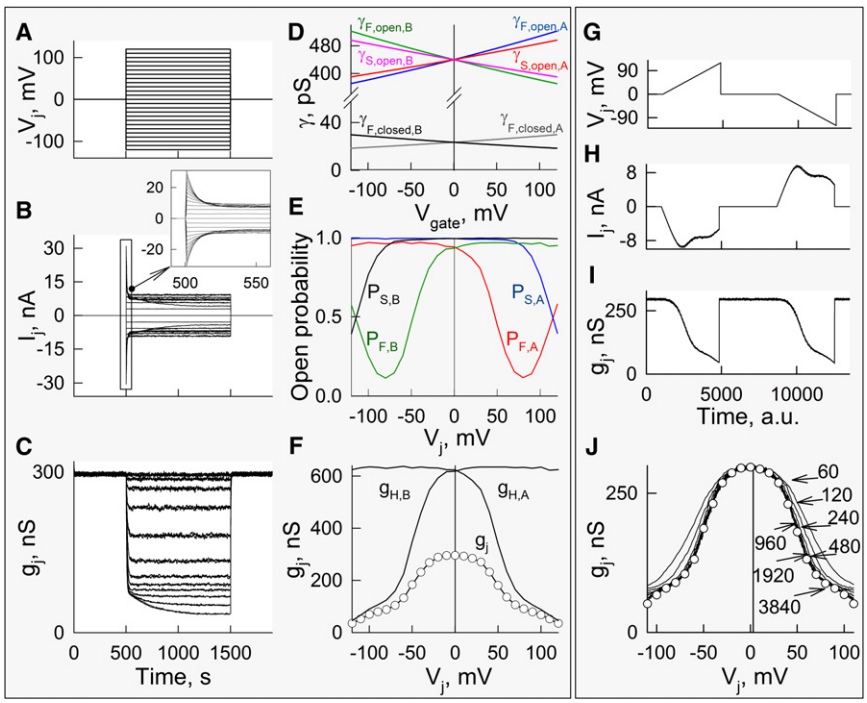

FIGURE 2 Simulation of V_j gating in a junction containing 3000 GJ channels. The parameters for the gates were chosen to be close to those of Cx43 (as shown in Table S1). We assumed that the conductance of each of the four gates in series at the open state is 440 pS and the residual conductance of the fast gate, $\gamma_{F,res}$, is equal to 25.9 pS, whereas the slow gates close fully. (*A–C*) I_j (*B*) and g_j (*C*) plots in response to a series of V_j steps that varied from −120 to 120 mV every 10 mV (*A*). (*D*) Dependence of $\gamma_{F,res}$, $\gamma_{F,open}$, and $\gamma_{S,o}$ on transgate voltage due to their I/V rectification ($R_{F,open} = R_{S,open} = 800$ mV and $R_{F,res} = 300$ mV). (*E*) Open probabilities of fast and slow gates in hemichannels A and B depending on V_j. (*F*) Conductance dependence on the voltage of GJs (g_j) and the left- and right-side hemichannels ($g_{H,A}$ and $g_{H,B}$) under steady-state conditions. (*G–J*) Simulation of V_j gating in the same junction as shown in *A–F* but in response to V_j ramps (*G*). (*H* and *I*) I_j and g_j traces. (*J*) g_j-V_j plots simulated with different durations of V_j ramps in arbitrary units (a.u.) of simulation time (60, 120, 240, 480, 960, 1920 and 3840 a.u.). The g_j-V_j plots simulated at V_j ramps of ≥960 a.u. practically overlap with the g_j-V_j plot simulated using V_j steps (*open circles*).

($g_{H,A}$) aCHs, depending on V_j, as well as $g_{j,ss}$-V_j dependence (*circles*) of GJs.

Fig. 2, *G–J*, show a simulation of V_j gating in the same junction as shown in Fig. 2, *A–F*, but in response to V_j ramps (*G*) instead of steps. Panels *H* and *I* show simulated I_j and g_j traces when the duration of each ramp was 3840 units of computer time, which we call arbitrary time units (a.u.). When we used voltage steps for $g_{j,ss}$-V_j plot measurements, we were able to determine whether I_j reached a steady state during V_j steps. Using the V_j-ramp protocol, it is less obvious whether ramps are long enough to measure g_js at their steady state. To test this, we examined $g_{j,ss}$-V_j plots at different durations of V_j ramps: 60, 120, 240, 480, 960, 1920, and 3840 a.u (Fig. 2 *J*). The $g_{j,ss}$-V_j plots measured with a duration of V_j ramps of $\geq$960 a.u. practically overlap and are very close to the $g_{j,ss}$-V_j plot from Fig. 2 *F* shown by open circles. When the duration of ramps was $\leq$480 a.u., $g_{j,ss}$-V_j plots demonstrated lower sensitivity to V_j due to a lack of time to reach the steady state. Thus, in real experiments, when voltage ramps are used for $g_{j,ss}$-V_j studies, the duration of V_j ramps should be at least ~2-fold longer than the duration of steps that satisfy conditions of the steady-state of I_j. The V_j-ramp protocol has advantages over V_j steps because it allows one to measure g_j continuously over the entire V_j range and takes >10-fold less time than the use of V_j steps.

Simulation of voltage gating in homotypic and heterotypic GJs at the single-channel level

Fig. 3 shows the simulation of I_j and g_j changes over time in a junction containing only one homotypic GJ channel using parameters shown in Table S1. Fig. 3 *A* shows I_j traces in response to three V_j steps of −30, −60, and −90 mV. It was assumed that both open and residual states do not rectify. I_j traces show that the open channel probability decays with V_j increase and the channel gates to two substates. For example, at $V_j = -90$ mV, when the channel is fully open, $I_j = 9.9$ pA. When one fast gate is closed to the residual state, then $I_j = 2$ pA, and we call this state the primary residual state. The arrows show the secondary residual state when two fast gates are closed, $I_j = 1.1$ pA. Closure of at least one of the slow gates results in zero conductance of the GJ channel. An overlay of g_j traces for all three voltage steps show that $\gamma_{open} = 110$ pS, whereas γ_{res} is equal to 22 pS for the primary residual state and 12 pS for the secondary residual state.

Fig. 3 *B* shows the g_j traces obtained by superposing g_js at V_j values of −30, −60, and −90 mV, in similarity to Fig. 3 *A*. All parameters are the same as in Fig. 3 *A*, but with the open and residual states exhibiting I/V rectification with $R_{F,open} = R_{S,open} = 800$ mV and $R_{F,res} = 300$ mV. Open channel conductances demonstrate three different levels of γ_{open} (109.9, 109.8, and 109.7 pS), which is due to the conductance rectification of open gates

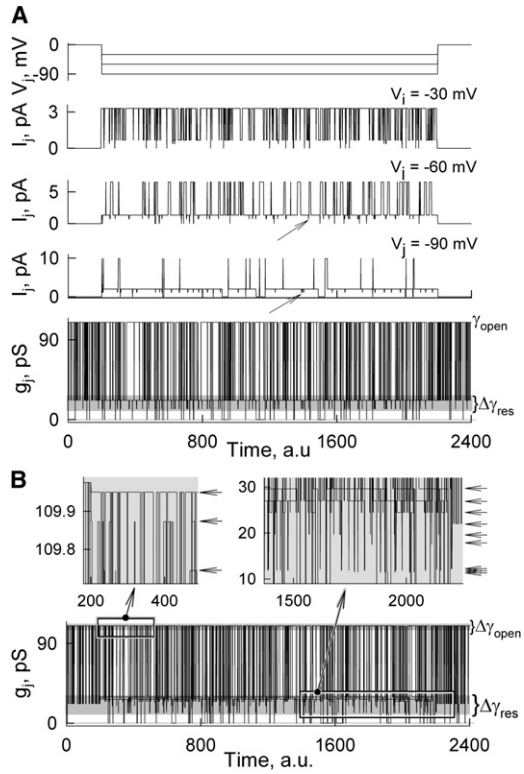

FIGURE 3 Simulation of voltage gating of the single homotypic GJ channel containing fast and slow gates in each hemichannel. Parameters of the gates are shown in Table S1. (*A*) I_j and g_j traces of nonrectifying channels ($R_{F,open}$, $R_{S,open}$, and $R_{F,res} \rightarrow \infty$) simulated at three V_j steps of −30, −60, and −100 mV. The g_j trace is an overlay of conductances calculated for all three voltage steps. (*B*) An overlay of g_j traces of the channel exhibiting rectification of fast and slow gates, $R_{F,open} = R_{S,open} = 600$ mV and $R_{F,res} = 200$ mV simulated at V_j steps of −30, −60, and −100 mV. The inset on the left demonstrates small variations (~0.2 pS) of γ_{open} depending on V_j; arrows show three values of γ_{open}. The inset on the right shows that in the presence of I/V rectification, three values of γ_{res} can be recorded at each V_j; thus, the use of three different voltage steps resulted in nine values of γ_{res} (*arrows*).

(see the *left inset*). The inset on the right shows multiple substates (*arrows*) with conductances in the range of 12–29 pS. When the fast gate in hemichannel A is closed, each of three V_j steps results in three different values of γ_{res} due to rectification. When the fast gate in hemichannel B, seeing V_j at an opposite polarity than hemichannel A, is closed, each of three V_j steps results in another set of γ_{res} values. Closing both fast gates also results in three values of γ_{res}. Therefore, I/V rectification leads to a significant number of substates (N_{Subst}), which theoretically equals $3 \times N_{Vj}$, where N_{Vj} is the number of used V_j steps. If V_j ramps are used instead of steps, then $N_{Subst} \rightarrow \infty$. During the I_j simulations shown in Fig. 3, Pτ, characterizing the probability that a gate will change the state during a discrete time interval, was selected to be relatively high (0.6), which resulted in a fast transition to the steady state, giving on average almost homogeneous I_j transitions over all durations of V_j steps.

In summary, for a homotypic nonrectifying GJ channel, we can expect a single conductance for γ_{open} and two conductances for γ_{res}, whereas for rectifying GJ channels we can expect a variety of γ_{open} and γ_{res}. However, variation of γ_{open} was ~90-fold lower than that of γ_{res} (~0.2 vs. 19 pS).

Fig. 4 *B* shows experimental data (modified from Fig. 9 in Bukauskas et al. (12)) of heterotypic GJs formed between a cell expressing wild-type Cx43 and a cell expressing Cx43-EGFP, in which the fast gate is inactivated or permanently open (schematic in *A*) (12). When the negative V_j step of −80 mV was applied to a cell expressing Cx43-EGFP, I_j showed the operation of two channels with gating transitions of 110 pS in magnitude between open and fully closed states. Both fast and slow gates of Cx43 exhibit a negative gating polarity (24). Consequently, a −80 mV step preferentially operates the Cx43-EGFP aHC. A V_j step of +80 mV induced gating transitions of ~85 pS between open and residual states (the *dashed line* indicates the level of I_j with both channels in the residual state). A transition of 110 pS indicating operation of the slow gate was rare, and absent in the example shown. Fig. 4 *C* shows simulated V_j and I_j traces (*gray*) in junctions containing two operational channels with $\gamma_{open} = 110$ pS measured experimentally in wtCx43 and Cx43-EGFP GJ channels (12). The simulated I_j record was obtained at $V_{F,o} = 25$ mV, $V_{S,o} = 60$ mV, $A_F = 0.11\ mV^{-1}$, and $A_S = 0.09\ mV^{-1}$. Under these conditions, at negative V_j, the step preferentially operates

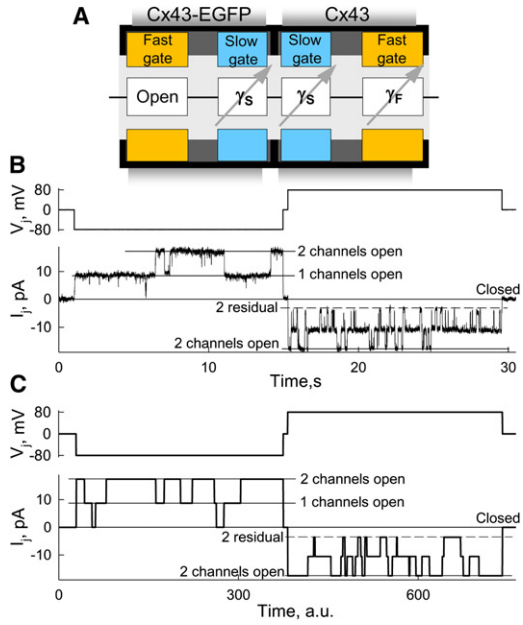

FIGURE 4 V_j gating of Cx43/Cx43-EGFP GJs. (*A*) Schematic of the Cx43-EGFP and Cx43 aHCs combined with the principal electrical scheme of the GJ channel. (*B*) Experimental I_j recording in response to V_j steps of −80 and +80 mV applied to a Cx43-EGFP cell (modified from Fig. 9 *B* in Bukauskas et al. (12)). (*C*) Simulated V_j and I_j traces (*gray*) in a junction composed of two GJ channels, each of which contains gates as shown in *A*.

the slow gate of Cx43-EGFP aHC. At a positive V_j step, the fast gate closes more often, leading to a reduction of voltage across the slow gates that lessens their operation and consequently full closures. Thus, this example illustrates how S16SM allows one to obtain a better understanding of experimentally observed phenomena.

Fitting of experimental data with S16SM using optimization algorithms

Our main goal in developing S16SM was to use it to fit experimental data for estimating the gating parameters of GJ channels. The parameters of the model can be changed manually to find the best fit between experimental and simulated $g_{j,ss}$-V_j plots based on visual or least-square or modulus difference criteria; we prefer to use the modulus difference. However, S16SM includes 12 variable parameters (six per gate) for homotypic GJ channels (if the $g_{j,ss}$-V_j plot is indeed symmetric to the *Y* axis at $X = 0$), and 24 for heterotypic GJ channels. Cells of the same pair can differ slightly in ionic balance, pH_i, etc., which may cause some asymmetry in $g_{j,ss}$-V_j dependence and requires global optimization for all four gates. Thus, manual fitting would be practically impossible and require the use of global optimization algorithms, which originally were elaborated for applications such as financial models and molecular-dynamics simulations. These algorithms are based on the Bayesian approach to filter the stochastic component and smooth small local minima while searching for the global minimum (25–27). This is important for the S16SM model because the least modulus difference is a multimodal stochastic function of unknown parameters. Conveniently, some parameters are known or predictable, e.g., $\gamma_{S,closed} = 0$ (consequently, the value of $R_{S,closed}$ also can be excluded from the optimization). Furthermore, $\gamma_{F,open}$ and $\gamma_{S,open}$ can be approximated from γ_{open} of the GJ channel, allowing for a further reduction in the number of variable parameters. However, very little is known about the rectification of unitary conductances of gates, as well as $\gamma_{F,res}$, and they were always left as variable parameters whose values were evaluated during global optimization. We exploited several optimization algorithms, including Exkor (a version of the GCO using the Bayesian approach and applying the Wiener model), Monte Carlo (random generation of function evaluation points), and Bayes (a multidimensional version of the Bayesian approach to global optimization), which differ in efficiency. In this study, we performed the fitting using an Intel-Core2 Quad CPU processor at 2.83 GHz for the Exkor GCO algorithm, and a cluster containing 800 processors at the Albert Einstein College of Medicine for the Monte Carlo algorithm.

Fig. 5 *A* shows a normalized $g_{j,ss}$-V_j plot measured in a HeLaCx45 cell pair (*black*) and simulated (*gray*) $g_{j,ss}$ $g_{j,ss}$-V_j plot (*gray*) obtained during global optimization. The GCO algorithm guided changes of independent

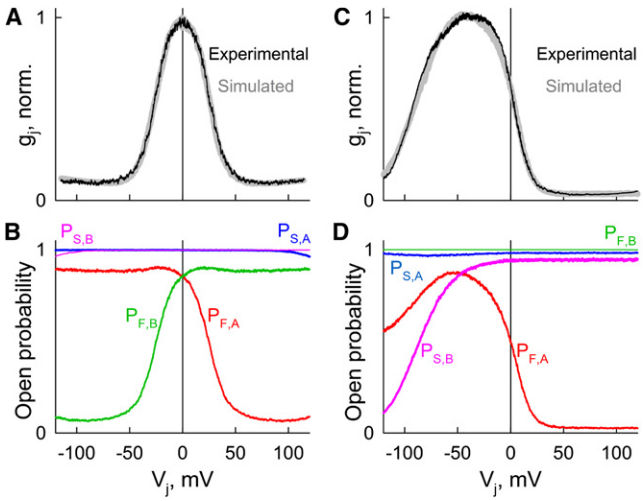

FIGURE 5 Global optimization of V_j gating of Cx45 homotypic (*A* and *B*) and Cx43-EGFP/Cx45 heterotypic (*C* and *D*) GJs. Experimental and simulated g_j-V_j plots in *A* and *C* are shown in black and gray, respectively. (*B* and *C*) Open probabilities of fast and slow gates residing in hemichannels A and B ($P_{F,A}$, $P_{S,A}$ and $P_{F,B}$, $P_{S,B}$, respectively) depending on V_j. P-V_j plots were simulated using values of parameters for fast and slow gates obtained during GCO.

parameters based on changes of the modulus difference between experimental and simulated curves. The fitting parameters were evaluated after 630 iterations during which was satisfied the least modulus difference criteria. Each iteration lasted ~5.2 s and involved simulation of the $g_{j,ss}$-V_j plot and calculation of the modulus difference. We obtained simulated $g_{j,ss}$-V_j plots assuming that the junction is composed of 2000 channels. Under these conditions, the noise of the simulated $g_{j,ss}$-V_j plot was close to that measured experimentally; a further increase in the number of channels increased the time of GCO but not its quality. At the starting point, the GCO algorithm requires a range of variable parameters that predictably include searchable values. Therefore, we used a relatively large range of values (shown in Table S2) based on reported unitary conductances and gating parameters of all known Cxs (3), as well as on our previous experience in global optimization. We assumed that $\gamma_{F,open}$ and $\gamma_{S,open}$ are equal to 128 pS; evaluation was based on the reported single-channel conductance of Cx45 (32 pS (24)) and on the postulate that conductances of fast and slow gates in the open/main state are equal, i.e., $\gamma_{F,open} = \gamma_{S,open} = 4\gamma_{open}$ (see above). As reported previously (24), the gating polarities of the fast and slow gates of Cx45 were negative. Therefore, there was no search for the gating polarity. Furthermore, during an initial GCO, we assumed that the $g_{j,ss}$-V_j relation is symmetric and all six variable parameters for the left and right hemichannels were identical. Global optimization took 54 min. Estimated values of the variable parameters are shown in Table S2.

However, as indicated above, nonhomogeneity of cells can lead to an asymmetry of the $g_{j,ss}$-V_j plot, which typically is relatively small, as shown in the experimental $g_{j,ss}$-V_j plot in Fig. 5 *A*. Consequently, we performed the second round of GCO assuming that parameters of the left and right hemichannels are not identical. In this case, the GCO included 12 variable parameters. Based on preliminary estimates, we defined new, at least ~5-fold narrower ranges of variable parameters. The final global optimization ended after ~950 iterations. If the value of one parameter was at the edge of a range of values, we would repeat the optimization by expanding this range. The new derived values of parameters are shown in Table S3 and the best-fitted $g_{j,ss}$-V_j plot simulated using these parameters is shown in gray in Fig. 5 *A*. Movie S1 and Movie S2 show preliminary and final GCOs (the experimental $g_{j,ss}$-V_j plot is in black, variable $g_{j,ss}$-V_j plots are in red, and the blue $g_{j,ss}$-V_j plot shows an intermediate best fit that gradually approaches the final $g_{j,ss}$-V_j plot). In total, the fitting process included 630 iterations for the coarse GCO and 950 iterations for the final GCO, and lasted ~2.28 h.

Fig. 5 *B* shows the best-fitted open probabilities of fast and slow gates residing in hemichannels A and B ($P_{F,A}$, $P_{S,A}$ and $P_{F,B}$, $P_{S,B}$, respectively) depending on V_j. P-V_j plots show that voltage gating is preferentially defined by fast gates, and that the open probability of GJ channels at $V_j = 0$ mV ($P_{Vj} = 0$) is ~0.7 ($P_{F,A} \cdot P_{S,A} \cdot P_{F,B} \cdot P_{S,B} = 0.85 \cdot 0.99 \cdot 0.85 \cdot 0.99 = \sim 0.7$), i.e., at $V_j = \sim 0$ channels are under an intense gating, resulting in ~30% of functional channels being closed at any given time.

Fig. 5, *C* and *D*, show the global optimization of a Cx43-EGFP/Cx45 heterotypic junction performed from an experimental $g_{j,ss}$-V_j plot shown in black (Fig. 5 *C*). We used the same strategy as for Cx45 homotypic GJs, but performed the initial and final GCOs assuming that parameters of aHCs A and B are different. The unitary conductances of fast and slow gates in Cx45 aHC, $\gamma_{F,open}$ and $\gamma_{S,open}$, equal 128 pS, i.e., they are the same as those used for Cx45 homotypic GJs. In accordance with assumptions made during simulation of Cx43/Cx43-EGFP GJs, $\gamma_{S,open}$ of Cx43-EGFP was equal to 440 pS. According to Bukauskas et al. (12), the fast gate of Cx43-EGFP is inactivated, i.e., permanently open with a conductance of 440 pS (Table S4). Consequently, after 1680 iterations, the global optimization resulted in the $g_{j,ss}$-V_j plot shown in Fig. 5 *C* in gray. Fig. 5 *D* shows the open probabilities of fast and slow gates residing in hemichannels A and B depending on V_j obtained using the fitted parameters shown in Table S4. P-V_j plots show that voltage gating at $V_j = 0$ is preferentially defined by the fast gate of Cx45, whereas g_j decay at negative V_j values depends on operation of the slow gate of Cx43-EGFP and the fast gate of Cx45. The decrease in $P_{F,A}$ at negative V_j values is due to the fact that when the slow gate of Cx43 closes, all V_j drops across it and voltage across the Cx45 fast gate becomes close to zero, at which point its open probability is substantially <1. Therefore, at higher negative V_j values, when more Cx43 gates close, more

Cx45 gates also close, resulting in the unexpected $P_{F,A}$ decrease.

The final values of variable parameters obtained during GCO are shown in Table S4. Movie S3 shows all 1680 iterations of the GCO resulting in the best fit of the experimental $g_{j,ss}$-V_j plot (the colors of the $g_{j,ss}$-V_j plots are the same as in Movie S1 and Movie S2). In total, the fitting process lasted ~2.42 h. It is important to note that experimental $g_{j,ss}$-V_j plots contain errors of different origins and this can explain, at least in part, nonideal GCOs.

DISCUSSION

Using S4SM, we were able to show that changes in $V_{F,o}$ can to a large degree explain the experimentally measured pH-dependent modulation of g_j in Cx57 (20) and Cx45 (21), as well as the uncoupling effect of long-chain alkanols (22). S16SM extends those possibilities by accounting for the operation of all four gates instead of two. Fig. S3 illustrates how addition of the slow gate affects $g_{j,ss}$-V_j plots in a junction containing 1000 GJ channels (values of all parameters are shown in Table S5). I_j and g_j traces in different colors were obtained at $V_{S,o}$ equal to 60, 35, 15, −5, and −20 mV. The I_j trace (*B*) and $g_{j,ss}$-V_j plot (*C*) shown in black were obtained in the absence of an operation of the slow gate. The presented data show that a gradual reduction in $V_{S,o}$ decreases g_{min} to zero, narrows the $g_{j,ss}$-V_j plot, and finally leads to full uncoupling.

S16SM revealed that the ratio $\gamma_{F,res}/\gamma_{F,open}$ is ~4-fold smaller than the corresponding ratio of the GJ channel, $\gamma_{res}/\gamma_{open}$ (~1/20 vs. 1/5). This indicates that the fast gate closes the channel pore more than predicted from the $\gamma_{res}/\gamma_{open}$ ratio. This may create size-limited restrictions for macromolecules to permeate the channel at the residual state and explain why there is no permeability of the residual state to dyes that permeate the open state (19,28) while leaving a relatively high level of electrical coupling.

In S16SM, we took into consideration that the conductances of both fast and slow gates rectify. We show that a nonrectifying GJ channel has one conductance for γ_{open} and two conductances for γ_{res} (Fig. 3, *A* and *C*), whereas rectifying channels have a potential to exhibit multiple conductances of γ_{open} and γ_{res} (Fig. 3, *B* and *D*). Furthermore, γ_{res} varied in a much broader range than γ_{open}. Of interest, multiple substates arise despite the fact that $\gamma_{F,res}$ is constant. These data may at least in part explain multiple substates measured at the single GJ channel level (16–18). In contrast, rectification of $\gamma_{F,open}$ and $\gamma_{S,open}$ minimally affected the initial or instantaneous g_j (g_{in}) in homotypic GJs. If $\gamma_{F,open}$ of the left-side aHC increases, then $\gamma_{F,open}$ of the right-side aHC decreases, resulting in a very small change of g_j over V_j (*inset* in Fig. 3 *B*). Therefore, it is problematic to detect $\gamma_{F,o}$ rectification from g_{in}-V_j plots of homotypic GJs. Otherwise, in heterotypic GJs, the aHC with lower conductance dominates in defining g_j, and the GJ channel can exhibit well-expressed g_{in} rectification. The effect of $\gamma_{F,res}$ rectification on g_{min} is well expressed in homo- and heterotypic GJ channels because the highest fraction of V_j drops on the closed fast gate than on three other open gates. This explains the $g_{j,min}$ increase in Cx45 GJs at $V_j > 60$ mV (Fig. 5 *A*). These conclusions are in accordance with earlier modeling studies (9) and Fig. 7 *D* of Paulauskas et al. (15).

Previously, V_j-gating asymmetry of heterotypic junctions was commonly used to determine the gating polarity of Cxs assuming that V_j gating of heterotypic junctions is a derivative of the intrinsic gating properties of composing aHCs (29). It was assumed that aHCs preserve their V_j-gating polarity in homo- and heterotypic junctions, and that an asymmetry of V_j gating can help one find the gating polarity for each Cx of the pair. As reported previously, this may be true only if the conductances of the aHCs are equal (2,13,15). It is evident that a higher fraction of V_j will drop across an aHC with smaller conductance than across an aHC with higher conductance. Therefore, the $g_{j,ss}$-V_j plot of heterotypic GJs can be very different from that predicted from homotypic $g_{j,ss}$-V_j plots of composing Cxs if the influence of their unitary conductances is not accounted for. Furthermore, in earlier studies of gating polarity, it was assumed that each aHC contains one gate. The gating polarities of fast and slow gates can be the same, as in Cx43 and Cx45, or different, as was shown for Cx46 (2). Therefore, it became evident that we should revise the question related to gating polarity by defining the gating polarities of both fast and slow gates for each Cx isoform. We envision that S16SM will serve this purpose well by leaving the gating polarity as a variable parameter during global optimization. In a previous study (20), we used a similar approach to define the gating polarity of Cx57.

By fitting experimental $g_{j,ss}$-V_j plots using global optimization (see Fig. 5, Movie S1, Movie S2, and Movie S3), we were able to calculate the parameters of the gates, as well as their open probabilities, as functions of V_j (Fig. 5 *B*), which cannot be measured directly by most advanced experimental approaches. We exploited several optimization algorithms, such as Monte Carlo, Exkor, and Byes (26), and found that each has both positive and negative aspects. The Monte Carlo algorithm is based on random selection of variable parameters and often requires >400,000 iterations (several days of computation using Intel-Core2 Quad CPU processor at 2.83 GHz) to achieve the best fit. This time was reduced to ~30 min when we used the cluster containing 800 processors. The Exkor algorithm allows one to derive the final fit using ~1000 iterations and a conventional desktop computer in a time range of ~40–150 min. We can see several ways to reduce the fitting time for practical use of S16SM. When we used a two-core computer and each core assigned 500 channels instead of 1000, the calculation time was reduced twofold. This suggests that the operation may parallelize well and time reduction should be proportional to the

number of processors. The fitting process is shorter when the range of free parameter values is narrower. Based on statistical data mining obtained during global optimization, with growing experience we will be able to more precisely formulate a range of free parameter values for different Cx isoforms. Thus, by reducing the number and range of variable parameters, and exploiting the most advanced algorithms of GCO and multicore computers, we should be able to reduce the fitting process substantially. Furthermore, using direct evaluation of a probabilistic distribution of 16 states under steady-state conditions instead of a stochastic approach allows one to obtain the $g_{j,ss}$-V_j dependence directly without calculating g_j dynamics in response to V_j protocols. Preliminary data show that this approach reduces GCO >100-fold, i.e., to a few minutes instead of 4–8 h.

The dynamics of g_j in experiments can be measured only when some V_j is applied, whereas S16SM allows one to follow changes of g_j at $V_j = 0$. This is highly important information for defining the dynamics of g_j before a V_j protocol is applied, or after g_j recovery subsequent to V_j gating. The model allows one to simulate V_j-gating properties at the single-channel level and to have an unlimited number of several different types of homo- or heterotypic GJ channels in the junctions. Finally, the proposed model applies to the study of voltage gating in unapposed hemichannels by eliminating one hemichannel from S16SM. Here, the number of variable parameters is reduced by half, which significantly increases the sureness of global optimization. Thus, this model provides a tool not only for studying the gating mechanisms of Cx-based channels but also for evaluating changes in gating parameters during the transition from normal/control to pathological conditions.

Although S16SM increases the potential of S4SM, there is still room for improvement. In the examples presented here, we used a.u., which is equal to a discrete time interval during which the model reevaluates the open probability for each gate and subsequently calculates the conductances of all channels. For example, in Fig. 4, a time interval of 31 s (*B*) was simulated with 750 a.u. (*C*). One can increase the number of Δt per real time unit by reducing the $P\tau$ parameter. Therefore, $P\tau$ can be left as a variable parameter in global optimization for both the $g_{j,ss}$-V_j plot and the I_j-time plots measured at V_j steps of different amplitude, which should increase confidence in the estimated gating parameters. Furthermore, S16SM assumes that the conductance of the GJ channel is composed of the conductances of four gates in series. Most likely, the gates occupy only a fraction of the pore, and the rest of the pore can be regarded as exhibiting a constant conductance, γ_{const}. If $\gamma_{const} >> \gamma_{F,open}$ and $\gamma_{S,open}$, it should not substantially affect V_j gating. The simulation using an S16SM that included γ_{const} showed a substantial reduction of V_j-gating sensitivity when γ_{const} was on the same order of $\gamma_{F,open}$ and $\gamma_{S,open}$ or below (see Fig. S4). The location of fast and slow gates, as well as γ_{const} relative to each other within each of two hemichannels, did not affect the $g_{j,ss}$-V_j plot. Our interest in γ_{const} was aroused by the demonstration by Dr. Verselis (Albert Einstein College of Medicine, personal communication, 2011) that reducing agents, which bind cysteine residing in mutated Cx46 uHC, significantly reduce not only unitary conductance but also voltage-sensitive gating. Changes in voltage gating can be explained by a direct effect of reducing agents on the gate, or more simply by obstruction of the pore and a decrease in γ_{const}. For example, Cx36 and mCx30.2 GJs exhibit the smallest unitary conductance (~10–15 pS) and lowest V_j-sensitive gating among 21 members of the Cx family (3). If Cx36 and mCx30.2 channels have a local obstruction/s in the pore, this could explain the low V_j-sensitive gating even if the intrinsic sensitivity to V_j of fast and slow gates remains relatively high. Thus, more detailed information about the functional properties of GJs should enhance the reliability of models that describe their gating processes.

SUPPORTING MATERIAL

Four figures, five tables, and three movies are available at http://www.biophysj.org/biophysj/supplemental/S0006-3495(12)00512-7.

We thank Dr. Michael Bennett, Dr. Vytas Verselis, and Dr. Mindaugas Pranevicius for helpful discussions during development of the model, and Angele Bukauskiene for excellent technical assistance.

This work was supported by National Institutes of Health grants R01NS072238 and RO1HL084464 to F.F.B.

REFERENCES

1. Bennett, M. V., and V. K. Verselis. 1992. Biophysics of gap junctions. *Semin. Cell Biol.* 3:29–47.
2. Bukauskas, F. F., and V. K. Verselis. 2004. Gap junction channel gating. *Biochim. Biophys. Acta.* 1662:42–60.
3. González, D., J. M. Gómez-Hernández, and L. C. Barrio. 2007. Molecular basis of voltage dependence of connexin channels: an integrative appraisal. *Prog. Biophys. Mol. Biol.* 94:66–106.
4. Harris, A. L., D. C. Spray, and M. V. L. Bennett. 1981. Kinetic properties of a voltage-dependent junctional conductance. *J. Gen. Physiol.* 77:95–117.
5. Bukauskas, F. F., and R. Weingart. 1994. Voltage-dependent gating of single gap junction channels in an insect cell line. *Biophys. J.* 67: 613–625.
6. Moreno, A. P., M. B. Rook, …, D. C. Spray. 1994. Gap junction channels: distinct voltage-sensitive and -insensitive conductance states. *Biophys. J.* 67:113–119.
7. Bukauskas, F. F., and C. Peracchia. 1997. Two distinct gating mechanisms in gap junction channels: CO2-sensitive and voltage-sensitive. *Biophys. J.* 72:2137–2142.
8. Banach, K., and R. Weingart. 2000. Voltage gating of Cx43 gap junction channels involves fast and slow current transitions. *Pflugers Arch.* 439:248–250.
9. Vogel, R., and R. Weingart. 1998. Mathematical model of vertebrate gap junctions derived from electrical measurements on homotypic and heterotypic channels. *J. Physiol.* 510:177–189.

10. Chen-Izu, Y., A. P. Moreno, and R. A. Spangler. 2001. Opposing gates model for voltage gating of gap junction channels. *Am. J. Physiol. Cell Physiol.* 281:C1604–C1613.

11. Ramanan, S. V., P. R. Brink, …, K. Banach. 1999. A three-state model for connexin37 gating kinetics. *Biophys. J.* 76:2520–2529.

12. Bukauskas, F. F., A. Bukauskiene, …, V. K. Verselis. 2001. Gating properties of gap junction channels assembled from connexin43 and connexin43 fused with green fluorescent protein. *Biophys. J.* 81: 137–152.

13. Rackauskas, M., M. M. Kreuzberg, …, F. F. Bukauskas. 2007. Gating properties of heterotypic gap junction channels formed of connexins 40, 43, and 45. *Biophys. J.* 92:1952–1965.

14. Trexler, E. B., M. V. Bennett, …, V. K. Verselis. 1996. Voltage gating and permeation in a gap junction hemichannel. *Proc. Natl. Acad. Sci. USA.* 93:5836–5841.

15. Paulauskas, N., M. Pranevicius, …, F. F. Bukauskas. 2009. A stochastic four-state model of contingent gating of gap junction channels containing two "fast" gates sensitive to transjunctional voltage. *Biophys. J.* 96:3936–3948.

16. Bukauskas, F. F., and R. Weingart. 1993. Multiple conductance states of newly formed single gap junction channels between insect cells. *Pflugers Arch.* 423:152–154.

17. Veenstra, R. D., H. Z. Wang, …, P. R. Brink. 1994. Connexin37 forms high conductance gap junction channels with subconductance state activity and selective dye and ionic permeabilities. *Biophys. J.* 66:1915–1928.

18. Bukauskas, F. F., C. Elfgang, …, R. Weingart. 1995. Biophysical properties of gap junction channels formed by mouse connexin40 in induced pairs of transfected human HeLa cells. *Biophys. J.* 68:2289–2298.

19. Bukauskas, F. F., A. Bukauskiene, and V. K. Verselis. 2002. Conductance and permeability of the residual state of connexin43 gap junction channels. *J. Gen. Physiol.* 119:171–185.

20. Palacios-Prado, N., S. Sonntag, …, F. F. Bukauskas. 2009. Gating, permselectivity and pH-dependent modulation of channels formed by connexin57, a major connexin of horizontal cells in the mouse retina. *J. Physiol.* 587:3251–3269.

21. Palacios-Prado, N., S. W. Briggs, …, F. F. Bukauskas. 2010. pH-dependent modulation of voltage gating in connexin45 homotypic and connexin45/connexin43 heterotypic gap junctions. *Proc. Natl. Acad. Sci. USA.* 107:9897–9902.

22. Skeberdis, V. A., L. Rimkute, …, F. F. Bukauskas. 2011. pH-dependent modulation of connexin-based gap junctional uncouplers. *J. Physiol.* 589:3495–3506.

23. Oh, S., J. B. Rubin, …, T. A. Bargiello. 1999. Molecular determinants of electrical rectification of single channel conductance in gap junctions formed by connexins 26 and 32. *J. Gen. Physiol.* 114:339–364.

24. Bukauskas, F. F., A. B. Angele, …, M. V. Bennett. 2002. Coupling asymmetry of heterotypic connexin 45/ connexin 43-EGFP gap junctions: properties of fast and slow gating mechanisms. *Proc. Natl. Acad. Sci. USA.* 99:7113–7118.

25. Mockus, J. 1994. Application of Bayesian approach to numerical methods of global and stochastic optimization. *J. Glob. Optim.* 4: 347–365.

26. Mockus, J. 2002. Bayesian heuristic approach to global optimization and examples. *J. Glob. Optim.* 22:191–203.

27. Floudas, C. A., and P. M. Pardalos, editors. 2009. Encyclopedia of Optimization. Springer, New York.

28. Qu, Y., and G. Dahl. 2002. Function of the voltage gate of gap junction channels: selective exclusion of molecules. *Proc. Natl. Acad. Sci. USA.* 99:697–702.

29. White, T. W., R. Bruzzone, …, D. A. Goodenough. 1994. Selective interactions among the multiple connexin proteins expressed in the vertebrate lens: the second extracellular domain is a determinant of compatibility between connexins. *J. Cell Biol.* 125:879–892.